PCCP

PAPER

Check for updates

Interactions of limonene with the water dimer†

S. Indira Murugachandran and M. Eugenia Sanz ![ORCID] *

The interactions of two molecules of water with the terpene limonene are characterised by chirped-pulse Fourier transform microwave spectroscopy. Seven isomers of limonene–$(H_2O)_2$ have been observed, and identified from the comparison of their experimental spectroscopic parameters with those predicted by computational methods. In all isomers a distorted water dimer binds to limonene through O–H$\cdots\pi$ and C–H$\cdots$O interactions, and shows a strong preference for interacting with equatorial conformations of limonene. O–H$\cdots\pi$ hydrogen bonds to both endocyclic and exocyclic double bonds of limonene are established. In one of the isomers the water dimer forms a bridge between the endocyclic and exocyclic double bonds of limonene. Our results help advance our understanding of the interactions of water with atmospheric compounds.

1. Introduction

Monoterpenes are a large group of natural compounds produced and released by plants to the atmosphere.[1,2] They are formed by condensation of two isoprene units, thus having the molecular formula $C_{10}H_{16}$, and can be open chain, monocyclic or bicyclic. By extension, the term monoterpene is sometimes applied to derivatives including alcohol, carbonyl or aldehyde groups, which are also known as monoterpenoids. Monoterpenes are components of essential oils and many show antifungal, antimicrobial and anti-inflammatory activities, among others.[1,2] Therefore, they play a key role in the development of new drugs.[1,2] Many monoterpenes are also used as perfumery ingredients due to their volatility.[3]

Once monoterpenes are in the atmosphere, they react quite quickly with ozone and radicals such as OH and NO_3, producing a range of oxidised products that are involved in the formation of secondary organic aerosol (SOA).[4–6] Water, which is the third most abundant species in the Earth's atmosphere,[7] has an active role in atmospheric processes and can modify the formation and composition of SOA.[7–13] Water has been found to participate in atmospheric reactions as a reactant, and to influence reaction rates acting as a catalyst or inhibitor through the formation of hydrogen-bonded complexes with other atmospheric molecules.[7–10,14] Some reactions may be relevant both in aqueous and gas phases, such as the water hydrolysis of aldehydes and ketones to form *gem*-diols,[15–18] and others may

be relevant at the surface of aqueous aerosol droplets, such as those involving ozone.[10] Understanding the interactions of water with other atmospheric compounds in the gas phase is essential to accurately modelling its effects and getting insight into the behaviour of more complicated systems like water droplets.

Limonene is one of the most abundant natural monoterpenes and a precursor of SOA.[6] It is a major constituent of the emissions of the boreal[19] and hemiboreal[20] forest, and of various trees used in urban development.[21] Limonene is formed of a cyclohexene ring with a methyl and isopropenyl group in para position. Four conformers of limonene, three equatorial and one axial, have been observed in the gas phase[22,23] (see Fig. 1). We have recently investigated the interactions of limonene with water using chirped pulse Fourier transform microwave (CP-FTMW) spectroscopy, and identified seven isomers of limonene–H_2O involving equatorial and axial limonene conformations and different water configurations.[24] Water showed a preference to bind to equatorial limonene through the endocyclic double bond.

Limonene–H_2O presented a ridged potential energy surface with many possible low-energy minima that display only small structural changes from one to another. Rotational spectroscopy was key to discriminate between different minima in limonene–H_2O thanks to its strong dependence on molecular structure and the use of isotopologue data, which allows determination of the atomic coordinates of the substituted isotopologue.[25] In addition, rotational spectroscopy yields the relative arrangement of the molecules in the complex and insight on the non-covalent interactions driving the preferred structures. This information is relevant to understand atmospheric nucleation, which occurs when stable clusters are formed spontaneously from gas-phase molecules. Furthermore, the gas-phase data obtained from rotational spectroscopy is directly comparable

Department of Chemistry, King's College London, London, SE1 1DB, UK.
E-mail: maria.sanz@kcl.ac.uk; Tel: +44 (0)2078487509

† Electronic supplementary information (ESI) available: Predicted spectroscopic parameters at different levels of theory, cartesian coordinates, measured frequencies, experimental spectroscopic parameters of the isotopic species and substitution coordinates. See DOI: https://doi.org/10.1039/d2cp04174j
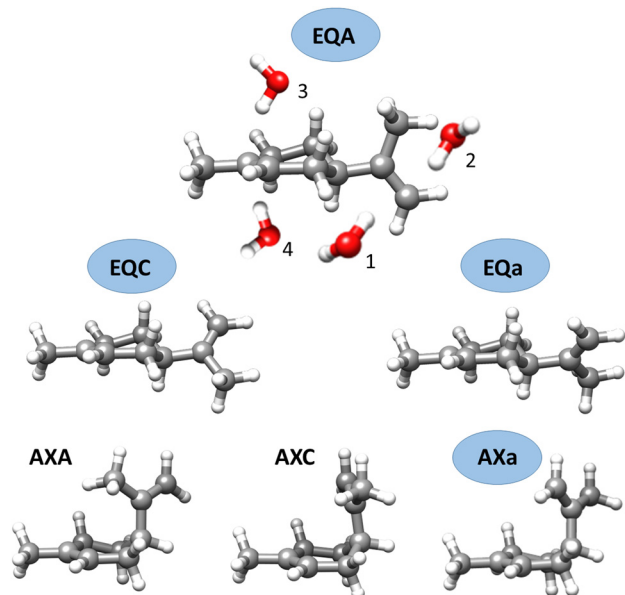
Fig. 1 The six possible conformers of limonene. Those observed experimentally have their label encircled in blue. The possible binding sites for water and their nomenclature are shown for the conformer at the top.

with predictions from theory, and can be used to benchmark different computational methods.

Using CP-FTMW spectroscopy in combination with computational calculations, we have examined further the interactions of limonene with water through the study of the limonene–$(H_2O)_2$ complex. We aimed to determine its preferred configurations and address several questions: would there be changes in the water binding preferences with respect to limonene–H_2O? Would the number of possible minima be reduced or increased when more water molecules bind to limonene? Would two water molecules bind limonene as a water dimer? Interactions of limonene with the water dimer could occur in the atmosphere. The water dimer was predicted to be in significant concentrations in the atmosphere by Goldman *et al.* in 2001,[26] and was observed at atmospherically relevant temperatures in 2013.[27] It has been found to react with the simplest Criegee intermediate.[28,29]

We have observed seven isomers of limonene–$(H_2O)_2$, which have been identified by carefully comparing the experimental and theoretical rotational constants, including those of ^{18}O isotopologues. Water maintains a preference to bind to equatorial conformers of limonene. A unique structure has been identified where the two water molecules link the endocyclic and exocyclic double bonds of limonene. Several theoretical methods have been used and benchmarked against the experimental data.

2. Methods

2.1. Experimental

The rotational spectrum of limonene–$(H_2O)_2$ was investigated in the 2–8 GHz range with our broadband rotational spectrometer, which has been described previously.[30,31] (*R*)-(+)-limonene (97%) was purchased from Sigma Aldrich and used without further

purification. Limonene, in a bespoke reservoir attached to the nozzle heated to *ca.* 304 K, and water, in an external reservoir in the injection line at room temperature, were seeded in neon at stagnation pressures of 6 bar. Optimal spectral intensities were obtained using molecular pulses of 1000 μs to create an adequate supersonic expansion in our vacuum chamber. The limonene–water complexes in each molecular pulse, formed at the throat of the nozzle by collisions, were polarised with 4 chirped microwave pulses of 4 μs duration varying linearly in frequency from 2–8 GHz and spaced 30 μs. Between microwave pulses, free induction decays (FID) were collected for 20 μs, amplified by a low noise amplifier, and then stored in the time domain in a fast oscilloscope. The final spectrum was obtained by coherently adding 1 M FIDs and using a fast Fourier transform algorithm to convert it to the frequency domain. Further experiments to observe ^{18}O isotopologues were performed with a $1:1$ mixture of $H_2{}^{16}O:H_2{}^{18}O$ (97%, Chem-Cruz) to obtain a final spectrum with 2.7 M FIDs.

2.2. Computational

The possible configurations of limonene–$(H_2O)_2$ were initially generated by considering the lower-energy limonene–H_2O complexes and adding an additional water molecule in different positions. A subsequent exploration of the potential energy surface (PES) of limonene–$(H_2O)_2$ was performed using the conformational sampling program CREST.[32] Both axial and equatorial conformers of limonene were included as starting structures for different CREST searches. The resulting structures were optimised using the B3LYP[33,34]-D3BJ[35,36] and MP2[37] methods with the 6-311++G(d,p) basis set within the Gaussian09[38] suite of programs, which yielded a total of 85 limonene–$(H_2O)_2$ isomers within 12 kJ mol^{-1}. Of these, 39 isomers were predicted within 4 kJ mol^{-1}. Their geometries were also optimised using wB97XD[39]/6-311++G(d,p), M06-2X[40]/6-311++G(d,p), and B2PLYP[41]-D3BJ/def2-TZVP methods. Their predicted rotational constants, dipole moments, relative energies with and without zero-point corrections, and BSSE binding energies (for MP2 and B3LYP-D3BJ) are given in Table 1, and Tables S1–S4 (ESI†).

The isomers of limonene–$(H_2O)_2$ have been labelled following the same nomenclature we used for the complexes of limonene with one water molecule (see Fig. 1). Limonene conformers are specified by the axial or equatorial position of the isopropenyl group and a letter indicating its dihedral angle with respect to the cyclohexene ring. The binding of the first water molecule to each side of the exocyclic double bond of limonene is indicated with the labels 1 and 2. Labels 3 and 4 indicate binding of the first water to the endocyclic double bond above or below the cyclohexene ring, respectively. Additional suffixes I, II, III, *etc.* indicate the different positions of the second water molecule in increasing order of energy.

3. Results and discussion

3.1. Potential energy surface

The diverse arrangements adopted by the water molecules, in addition to the configurations arising from limonene's conformations,

26530 | *Phys. Chem. Chem. Phys.*, 2022, **24**, 26529–26538

This journal is © the Owner Societies 2022

Table 1 Experimental and theoretical spectroscopic parameters of the observed species of limonene–$(H_2O)_2$

Parameter	Isomer 1 Experimental	EQA-3-II B3LYP[g]	MP2[h]	Isomer 2 Experimental	EQA-4-II B3LYP	MP2	Isomer 3 Experimental	EQC-4-I B3LYP	MP2
A^a (MHz)	947.0945(15)[f]	959.3	966.6	967.27928(59)	1012.1	1001.5	922.2727(17)	964.3	962.9
B (MHz)	597.89778(29)	607.0	606.5	578.59179(32)	570.3	577.9	604.06009(25)	605.5	603.5
C (MHz)	432.15280(24)	441.1	444.7	461.47508(29)	471.7	472.0	436.70875(20)	445.6	450.4
κ	−0.36	−0.36	−0.36	−0.54	−0.64	−0.60	−0.31	−0.38	−0.40
Δ_J (kHz)	0.0928(18)	0.0305	0.0375	0.1642(35)	0.0729	0.0697	0.0595(21)	0.0304	0.0370
Δ_{JK} (kHz)	0.437(13)	0.1159	0.1534	0.943(25)	−0.2085	−0.0610	0.8605(98)	−0.2181	−0.3059
Δ_K (kHz)	—	0.3506	0.3987	—	0.5159	0.3968	—	0.5698	0.6088
δ_J (kHz)	0.0350(15)	0.0034	0.0028	0.0413(17)	0.0182	0.0147	−0.0060(12)	−0.0010	−0.0040
δ_K (kHz)	—	0.1395	0.1578	0.847(41)	0.2063	0.1974	0.440(17)	0.2776	0.2885
μ_a^b (D)	Y	−2.9	−3.0	Y	−0.8	−0.9	Y	−3.0	−2.9
μ_b (D)	N	0.3	0.2	Y	−0.8	−0.5	N	−0.1	−0.1
μ_c (D)	N	0.5	0.0	Y	−1.3	−1.5	N	−0.5	−0.6
σ^c (kHz)	2.6	—	—	4.8	—	—	2.3	—	—
N^d	41	—	—	65	—	—	46	—	—
ΔE_0^e (cm^{-1})	—	27.2	0.0	—	88.7	62.1	—	80.5	149.7

Parameter	Isomer 4 Experimental	EQC-1-I B3LYP[g]	MP2[h]	Isomer 5 Experimental	EQC-2-I B3LYP	MP2
A^a (MHz)	1019.1339(12)[f]	1072.0	1058.6	1045.9874(58)	1075.2	1081.3
B (MHz)	580.01176(43)	579.3	581.3	535.88202(59)	541.4	538.8
C (MHz)	463.49138(36)	477.2	475.4	423.71543(49)	431.8	436.6
κ	−0.58	−0.66	−0.64	−0.64	−0.66	−0.68
Δ_J (kHz)	0.0116(34)	0.0174	0.0174	0.1081(25)	0.0878	0.0820
Δ_{JK} (kHz)	1.048(49)	−0.2319	−0.2970	—	0.6024	0.7058
Δ_K (kHz)	—	0.5635	0.6684	—	0.1786	0.1668
δ_J (kHz)	—	−0.0018	−0.0020	0.0238(29)	0.0195	0.0134
δ_K (kHz)	—	0.1828	0.2237	—	0.3885	0.3378
μ_a^b (D)	Y	2.9	2.6	Y	1.7	1.8
μ_b (D)	Y	2.2	2.5	N	−0.4	0.0
μ_c (D)	N	0.1	0.2	N	0.6	0.9
σ^c (kHz)	6.5	—	—	4.7	—	—
N^d	41	—	—	33	—	—
ΔE_0^e (cm^{-1})	—	70.2	304.9	—	89.3	161.1

Parameter	Isomer 6 Experimental	EQa-4-I B3LYP[g]	MP2[h]	Isomer 7 Experimental	EQA-2-I B3LYP	MP2
A^a (MHz)	971.2636(13)	1010.0	1000.1	994.4739(14)[f]	1010.3	990.5
B (MHz)	585.47084(56)	578.0	589.5	556.66918(49)	565.9	566.5
C (MHz)	472.25591(48)	482.8	479.0	415.83179(41)	422.5	418.6
κ	−0.55	−0.64	−0.58	−0.51	−0.51	−0.48
Δ_J (kHz)	0.0929(73)	0.0672	0.0539	0.1060(60)	0.0837	0.09597
Δ_{JK} (kHz)	0.531(47)	−0.8438	−0.1618	—	0.9145	1.42098
Δ_K (kHz)	—	1.0883	0.4189	1.40(15)	0.1069	−0.02341
δ_J (kHz)	—	0.0113	0.0062	0.0216(32)	0.0057	0.01959
δ_K (kHz)	0.542(83)	0.6629	0.2880	0.147(50)	0.2026	0.19576
μ_a^b (D)	Y	1.4	1.4	Y	−1.7	−2.0
μ_b (D)	N	0.2	0.1	Y	1.0	1.2
μ_c (D)	Y	−1.0	−1.4	Y	1.1	0.8
σ^c (kHz)	7.7	—	—	7.3	—	—
N^d	40	—	—	59	—	—
ΔE_0^e (cm^{-1})	—	123.3	156.7	—	129.5	267.1

[a] A, B and C are the rotational constants; κ is Ray's asymmetry parameter, Δ_J, Δ_{JK}, Δ_K, δ_J and δ_K are the quartic centrifugal distortion constants. [b] μ_a, μ_b and μ_c are the electric dipole moments along the principal inertial axes. Y/N indicates whether a-, b- or c-type transitions have been observed or not. [c] Rms deviation of the fit. [d] Number of rotational transitions included in the fit. [e] Relative energies including zero-point corrections. [f] Standard error in parentheses in units of the last digit. [g] B3LYP-D3BJ/6-311++G(d,p) level of theory. [h] MP2/6-311++G(d,p) level of theory.

give rise to a huge number of possible low-energy structures resulting in a very corrugated and intricate PES for limonene–$(H_2O)_2$.

From our previous investigation of limonene–H_2O,[24] water primarily interacts with limonene through an O–H···π hydrogen bond to either the endocyclic or exocyclic double bonds.

The second water molecule can bind to limonene or to the first water molecule. Structures where water binds to limonene without forming a water dimer have an energy penalty of about 18 kJ mol^{-1}, so all low-energy limonene–$(H_2O)_2$ complexes involve a water dimer interacting with limonene. Upon binding to limonene, the water dimer can adopt several configurations

This journal is © the Owner Societies 2022

Phys. Chem. Chem. Phys., 2022, **24**, 26529–26538 | **26531**

depending on the arrangement of the hydrogen atoms and the lone pair involved in the O–H···O hydrogen bond between the two water molecules (see Table 1). This gives rise to structurally similar sets of isomers, with the same limonene conformation and same location for the O–H···π bond but different configurations of the water dimer.

In addition to the O–H···π and O–H···O hydrogen bonds mentioned above, the lower-energy limonene–$(H_2O)_2$ structures show C–H···O interactions between the second water molecule and limonene that further anchor the former to the latter. Limonene–$(H_2O)_2$ structures without C–H···O interactions are predicted above 12.2 kJ mol^{-1}.

The above traits are common to all the calculation methods. However, there are differences in the energy ordering of the isomers (Tables S1–S4, ESI†). Considering the relative energies including zero-point corrections, the global minimum is predicted to be **EQA-3-II** by MP2 and B2PLYP-D3BJ, **EQA-3-I** by B3LYP-D3BJ or **EQC-1-I** by M06-2X and wB97XD. These isomers involve the two most abundant conformers of bare limonene, EQA and EQC.[22,23] It should be noted that all calculations methods predict a larger number of low-energy isomers involving EQA, the global minimum of limonene. MP2 consistently predicts isomers involving axial limonene at lower energies, ranging from 115 to 255 cm^{-1}, while M06-2X predict all of them above 400 cm^{-1}.

3.2. Rotational spectrum

The experimental rotational spectrum between 2–8 GHz of limonene–water is quite dense. After removal of the known transition frequencies assigned to bare limonene,[22,23] limonene–H_2O,[24] and water clusters,[42–45] many intense lines remained.

The majority of the low-energy isomers of limonene–$(H_2O)_2$ in Table 1 are prolate asymmetric tops predicted to have a large dipole moment along the a principal inertial axis. Therefore initial searches looked for R-branch a-type transitions of the series $J'_{0,J'} \leftarrow J''_{0,J''}$ and $J'_{1,J'} \leftarrow J''_{1,J''}$. Identification of experimental isomers was aided by using the spectral simulating and fitting program PGOPHER,[46] which incorporates AUTOFIT,[47] an automated fitting algorithm for molecular spectra. The computationally predicted A, B and C rotational constants along with the corresponding dipole moment components were used to simulate the rotational spectra of the lower-energy limonene–$(H_2O)_2$ isomers within PGOPHER. Initial automated searches yielded the first three isomers of limonene–$(H_2O)_2$, all of which were very intense in the spectrum. Removal of their lines from the spectrum and further careful and repeated searches led to the identification of four additional species.

Fits of measured transitions were performed using the semi-rigid rotor Hamiltonian of Watson[48] in the A reduction and I^r representation using Pickett's programs.[49] The initial sets of experimental rotational constants found using PGOPHER were used to predict and measure more rotational transitions, which were added to the fits. The final spectroscopic constants for the seven observed isomers of limonene–$(H_2O)_2$ are shown in

Fig. 2 Section of the rotational spectrum of limonene–$(H_2O)_2$ predicted at a rotational temperature of 1 K, showing the $5_{0,5} \leftarrow 4_{0,4}$ and $5_{1,5} \leftarrow 4_{1,4}$ rotational transitions for all observed isomers. Upper trace shows the experimental spectrum, lower trace shows the simulated spectrum using the experimentally determined rotational constants.

Table 1. A section of the experimental spectrum showing lines for the seven complexes is presented in Fig. 2.

No indication of methyl internal rotation splittings due to the two methyl tops of limonene was observed, as for limonene–H_2O. Predictions using XIAM[50] with B3LYP-D3BJ barrier heights of *ca.* 700 cm^{-1} (ring methyl) and 600 cm^{-1} (isopropenyl methyl) yield splittings of 5–60 kHz for observed transitions, smaller than the resolution of our experiment (*ca.* 100 kHz).

Assigning the observed isomers to specific dihydrate structures was particularly challenging due to the large number of low-energy structures predicted and the similarity of the experimental rotational constants to one another. Taking into account that the Ray's asymmetry parameters of the detected isomers have values between −0.31 and −0.64 (Table 1), we were able to disregard very prolate structures with $-1 < \kappa < -0.85$ and an asymmetric one with $\kappa = -0.15$, leaving 21 possible isomers.

In addition to the rotational constants, we considered the observed transition types, theoretical dipole moments, and the coordinates of the water oxygen atoms. For the latter, we ran experiments using enriched ^{18}O water, and observed the possible isotopologues, $^{18}O-^{16}O$, $^{16}O-^{18}O$ and $^{18}O-^{18}O$ for all isomers, except for isomer 4, for which the $^{18}O-^{18}O$ isotopologue was not detected. Their experimental spectroscopic parameters are shown in Tables S5–S11 (ESI†). From the differences in the moments of inertia between the parent species and the ^{18}O isotopologues, we obtained the coordinates a, b and c of the oxygen atoms in the principal inertial axis system using Kraitchman's equations[51] as implemented in the program KRA[52] (Table S12, ESI†).

Systematically considering the observed species, isomers 1 and 3 have very similar A, B and C rotational constants and only presented a-type spectrum. They could correspond to **EQA-3-II**, **EQA-3-I**, **EQA-3-IV**, or **EQC-4-I**, all of which have similar predicted rotational constants, a sizeable μ_a value and low μ_b and μ_c values. Considering the r_s coordinates for the oxygen atoms, isomer 3 can be unambiguously identified as **EQC-4-I**. Isomer 1 has the best agreement with the oxygen coordinates of **EQA-3-II**,

26532 | *Phys. Chem. Chem. Phys.*, 2022, **24**, 26529–26538

This journal is © the Owner Societies 2022

although it is also very close to those of **EQA-3-I**. These two isomers differ in the position of the second water molecule, but the change in position causes a change in axes that results in very similar oxygen coordinates. Considering the slightly closer agreement with **EQA-3-II**, and that this isomer is predicted to be lower in energy by more computational methods (MP2, B2PLYP-D3BJ and wB97XD), we have assigned isomer 1 to **EQA-3-II**.

Isomer 2 has spectroscopic parameters that could match those predicted for **EQA-4-II** or **EQC-4-I**. From the values of the r_s coordinates, isomer 2 can be unambiguously identified as **EQA-4-II**.

Isomer 4 can correspond to **EQC-3-I** or **EQC-1-I**, both of which have sizable μ_a and μ_b components, consistent with the observation of a- and b-type spectra. The structures of **EQC-3-I** and **EQC-1-I** are very similar except for the different direction of the O–H···O hydrogen bond, depending on which water molecule acts as a hydrogen bond donor to the other one, and the different positions of the hydrogens of the water molecules. These differences cause minimal changes in the predicted rotational constants and dipole moments. However, considering the oxygen coordinates, we have assigned isomer 4 to **EQC-1-I**. Moreover, all computational methods predict **EQC-1-I** as lower in energy.

Isomer 5 presents a similar situation to isomer 1. Comparison of the rotational constants and observed types of transitions points towards either **EQC-2-III** or **EQC-2-I**, which only differ in the position of the hydrogen atoms of the water molecule that binds to limonene though a O–H···π bond. The r_s coordinates of the oxygen atoms do not allow us to distinguish between the two structures, and therefore we have assigned isomer 5 as **EQC-2-I** as it is the complex predicted to be lowest in energy by all calculations.

Isomer 6, which shows a- and c-type spectrum, can correspond to **EQa-4-I** or **EQa-4-II**, and is assigned to **EQa-4-I** from the comparison of experimental and theoretical r_s coordinates of the oxygen atoms. The observation of a-, b- and c-type lines means that isomer 7 can only be **EQA-2-I**. The assignment is confirmed by the oxygen r_s coordinates. An overlay of the r_s coordinates with the equilibrium structures of all isomers are shown in Fig. 3.

Comparing experimental and theoretical rotational constants, MP2/6-311++G(d,p) and B3LYP-D3BJ/6-311++G(d,p) are the best performing methods in predicting the experimental rotational constants, with average deviations of 2.0% and 2.2%, respectively. wB97XD/6-311++G(d,p) and B2PLYP-D3BJ/def2-TZVP are somewhat worse, with average deviations of 2.8% and 3.0%, respectively, and the worst performing method is M06-2X/6-311++G(d,p) with an average deviation of 4.2%. All methods show larger differences for the A rotational constant, ranging from 2.9% for MP2 to 7.2% for M06-2X.

3.3. Isomer abundances and intermolecular interactions

The relative abundances of the seven observed isomers were estimated from measuring the intensities of common a-type transitions considering that line intensity is proportional to the square of the dipole moment in our experiment. The obtained abundances are **EQA-4-II** $\gg$ **EQA-3-II** $\approx$ **EQC-2-I** $\approx$ **EQC-4-I** $\approx$ **EQa-4-I** > **EQA-2-I** > **EQC-1-I**.

The experimental abundances are not consistent with the theoretical relative energies predicted by the different methods (Tables S1–S4, ESI†), or with ΔE(BSSE) interaction energies (Table S1, ESI†). The isomers with lower abundance, **EQC-1-I** and **EQA-2-I**, are predicted to have the higher relative energies of those observed by MP2. However, **EQC-1-I** is predicted by M06-2X and wB97XD to be the global minimum, and by B3LYP-D3BJ and B2PLYP-D3BJ to be one of the isomers with lower relative energy. **EQA-3-II** is predicted to be the global minimum by MP2 and B2PLYP-D3BJ, and to have a low relative energy by B3LYP-D3BJ and wB97XD. **EQA-4-II**, with the highest abundance, is however predicted to have a relative energy intermediate among those of observed isomers. The experimental abundances can be affected by relaxation processes of higher- to lower-energy isomers in the supersonic jet, which can occur if the barriers for interconversion are sufficiently low.[53,54] They can also be influenced by the initial abundances of the bare limonene conformers in the jet.

The observed isomers reveal a heavy bias towards structures involving the two most abundant conformers of bare limonene, EQA and EQC. In fact, all isomers have limonene in an equatorial conformation. Despite repeated searches, no limonene–$(H_2O)_2$ complexes with limonene in an axial conformation have been observed.

All isomers are stabilised by O–H···π hydrogen bonds between water and limonene, O–H···O hydrogen bonds between the two water molecules, and C–H···O interactions between the hydrogen atoms of limonene and the lone pairs of the oxygen atoms of water. Of the seven observed isomers, four exhibit one water molecule forming an O–H···π bond to the endocyclic double bond of limonene and two have one water molecule bonding to the exocyclic double bond. **EQC-1-I** is unique in that both water molecules bond to limonene, establishing two O–H···π hydrogen bonds rather than one and forming a bridge between the endocyclic and exocyclic double bonds. **EQC-1-I** also has secondary C–H···O hydrogen bonds between both water oxygens and the ring, differently to other isomers where only the second water molecule establishes C–H···O interactions.

The above non-covalent interactions between limonene and water can be visualised with the NCI method[55,56] and are shown in Fig. 3. The O–H···O bonds appear as strong attractive interactions with deep blue isosurfaces, and are pill-shaped, indicated their high directionality. In comparison, the O–H···π hydrogen bonds show lighter blue isosurfaces spreading along the C=C double bonds, indicating their slightly weaker attractive nature and lower directionality. C–H···O hydrogen bonds are less attractive and directional and appear as green isosurfaces.

To get further insight into the strength of the interactions at play we performed natural bonding orbital (NBO) analysis[57] (Tables S13–S19, ESI†) using Gaussian09.[38] The NBO results confirm that the strongest interaction in limonene–$(H_2O)_2$ is the O–H···O hydrogen bond, with values of 42.6–45.4 kJ mol^{-1},

This journal is © the Owner Societies 2022

Phys. Chem. Chem. Phys., 2022, **24**, 26529–26538 | **26533**

Fig. 3 B3LYP-D3BJ/6-311++G(d,p) structures of the observed isomers of limonene−$(H_2O)_2$ overlaid with the experimental substitution coordinates of the oxygens of water represented by green spheres. O–H···π bonds are shown with blue dotted lines, O···O in red and C–H···O in green. Intermolecular interactions (in Å) have been included along with the calculated distances at B3LYP-D3BJ (blue) and MP2 (red) level of theory. The NCI isosurfaces ($s = 0.5$) are showed, for values of sign(λ_2)ρ ranging from −0.025 to +0.025 a.u. Blue indicates strong attractive interactions, green indicates weak attractive interactions, and red indicates strong repulsive interactions.

except for **EQC-1-I** which shows a much weaker interaction of 30.1 kJ mol^{-1}. The second most attractive interaction is the O–H···π hydrogen bond, with values of 20.1–21.4 kJ mol^{-1}, again excluding **EQC-1-I**. **EQC-1-I** displays two O–H···π bonds, of 15.8 kJ mol^{-1} and 5.7 kJ mol^{-1} to the exocyclic and endocyclic double bonds of limonene, respectively. The overall energy associated to O–H···π interactions is thus 21.5 kJ mol^{-1} in **EQC-1-I**. The stronger O–H···π is that involving the exocyclic double bond of limonene, which was found to be slightly more electronegative than the endocyclic one.[24]

All isomers of limonene−$(H_2O)_2$ except **EQC-1-I** show hydrogen bond cooperativity due to the presence of sequential hydrogen bonds running in the same direction (homodromic), where all molecules act as both hydrogen atom donors and acceptors.[58,59] This strengthens individual hydrogen bonds by enhancing polarization. The much weaker O–H···O and O–H···π hydrogen bonds in **EQC-1-I** can be related to the presence of an antidromic hydrogen bond network where one

water molecule acts as a double hydrogen bond donor, and may explain its low abundance.

The effects of hydrogen bond cooperativity in limonene−$(H_2O)_2$ are evident if we compare the values of the NBO energies and theoretical bond lengths for the O–H···π bonds with those of limonene−H_2O.[24] The O–H···π hydrogen bonds in the mono-hydrate isomers were predicted by NBO analysis to have energies ranging 11.3–13.8 kJ mol^{-1}, about 63% lower than those in the dihydrates. Additionally, the O–H···π bond length in the monohydrates is longer (2.25–2.29 Å from B3LYP-D3BJ and 2.28–2.34 Å from MP2) than in the dihydrates (2.17–2.24 Å from B3LYP-D3BJ and 2.19–2.27 Å from MP2), excluding **EQC-1-I**.

The effects of cooperativity are also manifest in the O···O distances (Fig. 3), shorter than the 2.98(4) Å of the free water dimer,[60] except for isomer **EQC-1-I**, where there are non-sequential hydrogen bonds preventing cooperativity. Similar shortening of the O···O distance have been observed in other complexes of terpenoids with the water dimer.[61–66] The predicted

$\angle O_{w1}H_{w2}O_{w2}$ angles of all isomers are smaller than $180°$, most likely the result of optimising secondary C–H···O interactions.

The observation of seven isomers of limonene–$(H_2O)_2$ further confirms the ability of water to interact with limonene. No isomers with limonene in an axial conformation have been observed, indicating a stronger preference of the water dimer to bind to equatorial conformers of limonene than in limonene–H_2O. In the majority of the isomers observed, the first water molecule prefers to bind to the endocyclic double bond, similarly to limonene–H_2O.

4. Conclusions

Seven isomers of limonene–$(H_2O)_2$ have been identified from the analysis of its broadband rotational spectrum supported by computational calculations. The two water molecules bind to limonene as a distorted water dimer, establishing O–H···π and C–H···O hydrogen bonds with limonene, and O–H···O bonds between each other. Limonene prefers to adopt an equatorial conformation in the complexes. One limonene–$(H_2O)_2$ isomer shows the water dimer binding to both endocyclic and exocyclic double bonds of limonene, forming a bridge between them, but most isomers display O–H···π hydrogen bonds to the endocyclic double bond. Our study provides new data on O–H···π interactions and their interplay with other hydrogen bonds, of interest to model related clusters.

Limonene–$(H_2O)_2$ presents a very corrugated PES with many low-energy minima that in some cases only differ by small structural changes involving the water molecules. A combination of manual prediction of possible structures guided by chemical intuition as well as algorithm-driven searches was found optimal for a more complete mapping of the PES. In comparison with limonene–H_2O, the addition of a second water molecule greatly increases the complexity of the PES and the number of low-energy isomers with close relative energies.

Several computational methods have been applied to the investigation of limonene–$(H_2O)_2$ and benchmarked against experimental data. B3LYP-D3BJ and MP2 with the 6-311++G(d,p) basis set predicted rotational constants closer to the experimental ones. This is with the caveat that we are comparing equilibrium rotational constants (predicted A_e, B_e, C_e) with ground vibrational state ones (experimental A_0, B_0, C_0), because of the high computational cost of calculating vibrational corrections for molecular systems like limonene–$(H_2O)_2$. Theoretical results were inconsistent with respect to the global minimum structure and the relative energy ordering, which showcases the difficulties in describing a molecular system like limonene–$(H_2O)_2$, with a high number of configurations within a small energy range of 4 kJ mol^{-1}.

Humidity has been found to affect the products of limonene ozonolysis, although the mechanism is not clear.[12,67] The results presented here show that the water dimer readily interacts with limonene, and prefers to bind to the endocyclic double bond, which is also the preferred site for limonene ozonolysis.[68] Limonene–$(H_2O)_2$ displays the same preference as limonene–H_2O. Our data informs on the initial steps of water microsolvation of limonene and contributes to understanding possible interactions of limonene in the atmosphere.

Author contributions

Conceptualization, M. E. S.; investigation, S. I. M.; formal analysis, S. I. M. and M. E. S.; resources, M. E. S.; writing – original draft preparation, S. I. M. and M. E. S.; writing – review and editing, S. I. M. and M. E. S.; visualization, S. I. M. and M. E. S.; supervision, project administration, and funding acquisition, M. E. S.

Conflicts of interest

There are no conflicts to declare.

Notes and references

1 A. Koziol, A. Stryjewska, T. Librowski, K. Salat, M. Gawel, A. Moniczewski and S. Lochynski, An overview of the pharmacological properties and potential applications of natural monoterpenes, *Mini-Rev. Med. Chem.*, 2014, **14**, 1156–1168.

2 M. Zielińska-Błajet and J. Feder-Kubis, Monoterpenes and their derivatives-Recent development in biological and medical applications, *Int. J. Mol. Sci.*, 2020, **21**, 7078.

3 *The Chemistry of Fragrances*, ed. D. Pybus and C. Sell, Royal Society of Chemistry, Cambridge, 2nd edn, 2006.

4 M. Hallquist, J. C. Wenger, U. Baltensperger, Y. Rudich, D. Simpson, M. Claeys, J. Dommen, N. M. Donahue, C. George, A. H. Goldstein, J. F. Hamilton, H. Herrmann, T. Hoffmann, Y. Iinuma, M. Jang, M. E. Jenkin, J. L. Jimenez, A. Kiendler-Scharr, W. Maenhaut, G. McFiggans, T. F. Mentel, A. Monod, A. S. H. Prévôt, J. H. Seinfeld, J. D. Surratt, R. Szmigielski and J. Wildt, The formation, properties and impact of secondary organic aerosol: Current and emerging issues, *Atmos. Chem. Phys.*, 2009, **9**, 5155–5236.

5 J. H. Kroll and J. H. Seinfeld, Chemistry of secondary organic aerosol: Formation and evolution of low-volatility organics in the atmosphere, *Atmos. Environ.*, 2008, **42**, 3593–3624.

6 M. Kanakidou, J. H. Seinfeld, S. N. Pandis, I. Barnes, F. J. Dentener, M. C. Facchini, R. Van Dingenen, B. Ervens, A. Nenes, C. J. Nielsen, E. Swietlicki, J. P. Putaud,

This journal is © the Owner Societies 2022

Phys. Chem. Chem. Phys., 2022, **24**, 26529–26538 | **26535**

Y. Balkanski, S. Fuzzi, J. Horth, G. K. Moortgat, R. Winterhalter, C. E. L. Myhre, K. Tsigaridis, E. Vignati, E. G. Stephanou and J. Wilson, Organic aerosol and global climate modelling: a review, *Atmos. Chem. Phys.*, 2005, **5**, 1053–1123.

7 R. J. Buszek, J. S. Francisco and J. M. Anglada, Water effects on atmospheric reactions, *Int. Rev. Phys. Chem.*, 2011, **30**, 335–369.

8 V. Vaida, H. G. Kjaergaard and K. J. Feierabend, Hydrated complexes: relevance to atmospheric chemistry and climate, *Int. Rev. Phys. Chem.*, 2003, **22**, 203–219.

9 V. Vaida, Perspective: Water cluster mediated atmospheric chemistry, *J. Chem. Phys.*, 2011, **135**, 020901.

10 J. M. Anglada, G. J. Hoffman, L. V. Slipchenko, M. M. Costa, M. F. Ruiz-López and J. S. Francisco, Atmospheric significance of water clusters and ozone–water complexes, *J. Phys. Chem. A*, 2013, **117**, 10381–10396.

11 T. B. Nguyen, P. J. Roach, J. Laskin, A. Laskin and S. A. Nizkorodov, Effect of humidity on the composition of isoprene photooxidation secondary organic aerosol, *Atmos. Chem. Phys.*, 2011, **11**, 6931–6944.

12 B. Bonn, G. Schuster and G. K. Moortgat, Influence of water vapor on the process of new particle formation during monoterpene ozonolysis, *J. Phys. Chem. A*, 2002, **106**, 2869–2881.

13 B. Bonn and G. K. Moortgat, New particle formation during α- and β-pinene oxidation by O3, OH and NO3, and the influence of water vapour: Particle size distribution studies, *Atmos. Chem. Phys.*, 2002, **2**, 83–196.

14 E. G. Schnitzler, C. Badran and W. Jäger, Contrasting effects of water on the barriers to decarboxylation of two oxalic acid monohydrates: a combined rotational spectroscopic and ab initio study, *J. Phys. Chem. Lett.*, 2016, **7**, 1143–1147.

15 J. L. Axson, K. Takahashi, D. O. De Haan and V. Vaida, Gas-phase water-mediated equilibrium between methylglyoxal and its geminal diol, *Proc. Natl. Acad. Sci. U. S. A.*, 2010, **107**, 6687–6692.

16 M. K. Maroń, K. Takahashi, R. K. Shoemaker and V. Vaida, Hydration of pyruvic acid to its geminal-diol, 2,2-dihydroxypropanoic acid, in a water-restricted environment, *Chem. Phys. Lett.*, 2011, **513**, 184–190.

17 W. Li, A. Maris, C. Calabrese, I. Usabiaga, W. D. Geppert, L. Evangelisti and S. Melandri, Atmospherically relevant acrolein-water complexes: Spectroscopic evidence of aldehyde hydration and oxygen atom exchange, *Phys. Chem. Chem. Phys.*, 2019, **21**, 23559–23566.

18 E. Burevschi, I. Peña and M. E. Sanz, Geminal diol formation from the interaction of a ketone with water in the gas phase: structure and reactivity of cyclooctanone-$(H_2O)_{1,2}$ clusters, *J. Phys. Chem. Lett.*, 2021, **12**, 12419–12425.

19 H. Hakola, V. Tarvainen, A. P. Praplan, K. Jaars, M. Hemmilä, M. Kulmala, J. Bäck and H. Hellén, Terpenoid and carbonyl emissions from Norway spruce in Finland during the growing season, *Atmos. Chem. Phys.*, 2017, **17**, 3357–3370.

20 S. M. Noe, K. Hüve, Ü. Niinemets and L. Copolovici, Seasonal variation in vertical volatile compounds air concentrations within a remote hemiboreal mixed forest, *Atmos. Chem. Phys.*, 2012, **12**, 3909–3926.

21 A. J. Curtis, D. Helmig, C. Baroch, R. Daly and S. Davis, Biogenic volatile organic compound emissions from nine tree species used in an urban tree-planting program, *Atmos. Environ.*, 2014, **95**, 634–643.

22 J. R. A. Moreno, T. R. Huet and J. J. L. González, Conformational relaxation of S-(+)-carvone and R-(+)-limonene studied by microwave Fourier transform spectroscopy and quantum chemical calculations, *Struct. Chem.*, 2013, **24**, 1163–1170.

23 D. Loru, A. Vigorito, A. F. M. Santos, J. Tang and M. E. Sanz, The axial/equatorial conformational landscape and intramolecular dispersion: New insights from the rotational spectra of monoterpenoids, *Phys. Chem. Chem. Phys.*, 2019, **21**, 26111–26116.

24 S. I. Murugachandran, J. Tang, I. Peña, D. Loru and M. E. Sanz, New insights into secondary organic aerosol formation: water binding to limonene, *J. Phys. Chem. Lett.*, 2021, 1081–1086.

25 D. Loru, I. Peña and M. E. Sanz, The role of secondary interactions on the preferred conformers of the fenchone-ethanol complex, *Phys. Chem. Chem. Phys.*, 2019, **21**, 2938–2945.

26 N. Goldman, R. S. Fellers, C. Leforestier and R. J. Saykally, Water dimers in the atmosphere: equilibrium constant for water dimerization from the VRT(ASP-W) potential surface, *J. Phys. Chem. A*, 2001, **105**, 515–519.

27 M. Y. Tretyakov, E. A. Serov, M. A. Koshelev, V. V. Parshin and A. F. Krupnov, Water dimer rotationally resolved millimeter-wave spectrum observation at room temperature, *Phys. Rev. Lett.*, 2013, **110**, 93001.

28 T. R. Lewis, M. A. Blitz, D. E. Heard and P. W. Seakins, Direct evidence for a substantive reaction between the Criegee intermediate{,} CH2OO{,} and the water vapour dimer, *Phys. Chem. Chem. Phys.*, 2015, **17**, 4859–4863.

29 M. C. Smith, C.-H. Chang, W. Chao, L.-C. Lin, K. Takahashi, K. A. Boering and J. J.-M. Lin, Strong Negative Temperature Dependence of the Simplest Criegee Intermediate CH2OO Reaction with Water Dimer, *J. Phys. Chem. Lett.*, 2015, **6**, 2708–2713.

30 D. Loru, M. A. Bermúdez and M. E. Sanz, Structure of fenchone by broadband rotational spectroscopy Structure of fenchone by broadband rotational spectroscopy, *J. Chem. Phys.*, 2016, **145**, 074311–074318.

31 D. Loru, I. Peña and M. E. Sanz, Ethanol dimer: Observation of three new conformers by broadband rotational spectroscopy, *J. Mol. Spectrosc.*, 2017, **335**, 93–101.

32 P. Pracht, F. Bohle and S. Grimme, Automated exploration of the low-energy chemical space with fast quantum chemical methods, *Phys. Chem. Chem. Phys.*, 2020, **22**, 7169–7192.

33 C. Lee, W. Yang and R. G. Parr, Development of the Colle-Salvetti correlation-energy formula into a functional of the electron density, *Phys. Rev. B: Condens. Matter Mater. Phys.*, 1988, **37**, 785–789.

34 A. D. Becke, A new mixing of Hartree–Fock and local density-functional theories, *J. Chem. Phys.*, 1993, **98**, 1372–1377.

26536 | *Phys. Chem. Chem. Phys.*, 2022, **24**, 26529–26538

This journal is © the Owner Societies 2022

35 S. Grimme, J. Antony, S. Ehrlich and H. Krieg, A consistent and accurate ab initio parametrization of density functional dispersion correction (DFT-D) for the 94 elements H-Pu, *J. Chem. Phys.*, 2010, **132**, 154104.

36 S. Grimme, S. Ehrlich and L. Goerigk, Effect of the damping function in dispersion corrected density functional theory, *J. Comput. Chem.*, 2011, **32**, 1456–1465.

37 C. Møller and M. S. Plesset, Note on an approximation treatment for many-electron systems, *Phys. Rev.*, 1934, **46**, 618–622.

38 M. J. Frisch, G. W. Trucks, H. B. Schlegel, G. E. Scuseria, M. A. Robb, J. R. Cheeseman, G. Scalmani, V. Barone, B. Mennucci, G. A. Petersson, H. Nakatsuji, M. Caricato, X. Li, H. P. Hratchian, A. F. Izmaylov, J. Bloino, G. Zheng, J. L. Sonnenberg, M. Hada, M. Ehara, K. Toyota, R. Fukuda, J. Hasegawa, M. Ishida, T. Nakajima, Y. Honda, O. Kitao, H. Nakai, T. Vreven, J. A. Montgomery Jr., J. E. Peralta, F. Ogliaro, M. Bearpark, J. J. Heyd, E. Brothers, K. N. Kudin, V. N. Staroverov, R. Kobayashi, J. Normand, K. Raghavachari, A. Rendell, J. C. Burant, S. S. Iyengar, J. Tomasi, M. Cossi, N. Rega, J. M. Millam, M. Klene, J. E. Knox, J. B. Cross, V. Bakken, C. Adamo, J. Jaramillo, R. Gomperts, R. E. Stratmann, O. Yazyev, A. J. Austin, R. Cammi, C. Pomelli, J. W. Ochterski, R. L. Martin, K. Morokuma, V. G. Zakrzewski, G. A. Voth, P. Salvador, J. J. Dannenberg, S. Dapprich, A. D. Daniels, Ö. Farkas, J. B. Foresman, J. V. Ortiz, J. Cioslowski and D. J. Fox, *Gaussian 09 Revis. E.01*, 2010.

39 J. Da Chai and M. Head-Gordon, Long-range corrected hybrid density functionals with damped atom-atom dispersion corrections, *Phys. Chem. Chem. Phys.*, 2008, **10**, 6615–6620.

40 Y. Zhao and D. G. Truhlar, The M06 suite of density functionals for main group thermochemistry, thermochemical kinetics, noncovalent interactions, excited states, and transition elements: Two new functionals and systematic testing of four M06-class functionals and 12 other function, *Theor. Chem. Acc.*, 2008, **120**, 215–241.

41 S. Grimme, Semiempirical hybrid density functional with perturbative second-order correlation, *J. Chem. Phys.*, 2006, **124**, 034108.

42 C. Pérez, M. T. Muckle, D. P. Zaleski, N. A. Seifert, B. Temelso, G. C. Shields, Z. Kisiel and B. H. Pate, Structures of cage, prism, and book isomers of water hexamer from broadband rotational spectroscopy, *Science*, 2012, **336**, 897–902.

43 C. Pérez, S. Lobsiger, N. A. Seifert, D. P. Zaleski, B. Temelso, G. C. Shields, Z. Kisiel and B. H. Pate, Broadband Fourier transform rotational spectroscopy for structure determination: The water heptamer, *Chem. Phys. Lett.*, 2013, **571**, 1–15.

44 C. Pérez, D. P. Zaleski, N. A. Seifert, B. Temelso, G. C. Shields, Z. Kisiel and B. H. Pate, Hydrogen bond cooperativity and the three-dimensional structures of water nonamers and decamers, *Angew. Chem., Int. Ed.*, 2014, **53**, 14368–14372.

45 J. O. Richardson, C. Pérez, S. Lobsiger, A. A. Reid, B. Temelso, G. C. Shields, Z. Kisiel, D. J. Wales, B. H. Pate and S. C. Althorpe, Concerted hydrogen-bond breaking by quantum tunneling in the water hexamer prism, *Science*, 2016, **351**, 1310–1313.

46 C. M. Western and B. E. Billinghurst, Automatic and semi-automatic assignment and fitting of spectra with PGO-PHER, *Phys. Chem. Chem. Phys.*, 2019, **21**, 13986–13999.

47 N. A. Seifert, I. A. Finneran, C. Perez, D. P. Zaleski, J. L. Neill, A. L. Steber, R. D. Suenram, A. Lesarri, S. T. Shipman and B. H. Pate, AUTOFIT, an automated fitting tool for broadband rotational spectra, and applications to 1-hexanal, *J. Mol. Spectrosc.*, 2015, **312**, 13–21.

48 J. K. G. Watson, in *Vibrational spectra and structure, A series of advances*, ed. J. R. Durig, 1977, vol. 6, pp. 1–89.

49 H. M. Pickett, The fitting and prediction of vibration-rotation spectra with spin interactions, *J. Mol. Spectrosc.*, 1991, **148**, 371–377.

50 H. Hartwig and H. Dreizler, The microwave spectrum of trans-2,3-dimethyloxirane in torsional excited states, *Z. Naturforsch., A: Phys. Sci.*, 1996, **51**, 923–932.

51 J. Kraitchman, Determination of molecular structure from microwave spectroscopic data, *Am. J. Phys.*, 1953, **21**, 17–24.

52 Z. Kisiel, PROSPE – Programs for ROtational SPEctroscopy, *Spectroscopy from Space*, 2001, 91–106.

53 R. S. Ruoff, T. D. Klots, T. Emilsson and H. S. Gutowsky, Relaxation of conformers and isomers in seeded supersonic jets of inert gases, *J. Chem. Phys.*, 1990, **93**, 3142–3150.

54 G. M. Florio, R. A. Christie, K. D. Jordan and T. S. Zwier, Conformational preferences of jet-cooled melatonin: Probing *trans*- and *cis*-amide regions of the potential energy surface, *J. Am. Chem. Soc.*, 2002, **124**, 10236–10247.

55 E. R. Johnson, S. Keinan, P. Mori-Sánchez, J. Contreras-García, A. J. Cohen and W. Yang, Revealing noncovalent interactions, *J. Am. Chem. Soc.*, 2010, **132**, 6498–6506.

56 R. Chaudret, B. De Courcy, J. Contreras-García, E. Gloaguen, A. Zehnacker-Rentien, M. Mons and J. P. Piquemal, Unraveling non-covalent interactions within flexible biomolecules: From electron density topology to gas phase spectroscopy, *Phys. Chem. Chem. Phys.*, 2014, **16**, 9876–9891.

57 A. E. Reed, L. A. Curtiss and F. Weinhold, Intermolecular interactions from a natural bond orbital, donor-acceptor viewpoint, *Chem. Rev.*, 1988, **88**, 899–926.

58 W. Saenger, Circular hydrogen bonds, *Nature*, 1979, **279**, 343–344.

59 G. A. Jeffrey, *An introduction to hydrogen bonding*, Oxford University Press, 1997.

60 T. R. Dyke, K. M. Mack and J. S. Muenter, The structure of water dimer from molecular beam electric resonance spectroscopy, *J. Chem. Phys.*, 1977, **66**, 498–510.

61 C. Pérez, A. Krin, A. L. Steber, J. C. López, Z. Kisiel and M. Schnell, Wetting camphor: multi-isotopic substitution identifies the complementary roles of hydrogen bonding and dispersive forces, *J. Phys. Chem. Lett.*, 2016, **7**, 154–160.

62 M. Chrayteh, A. Savoia, T. R. Huet and P. Dréan, Microhydration of verbenone: How the chain of water molecules adapts its structure to the host molecule, *Phys. Chem. Chem. Phys.*, 2020, **22**, 5855–5864.

This journal is © the Owner Societies 2022

Phys. Chem. Chem. Phys., 2022, **24**, 26529–26538 | **26537**

63 M. Chrayteh, T. R. Huet and P. Dréan, Gas-Phase Hydration of Perillaldehyde Investigated by Microwave Spectroscopy Assisted by Computational Chemistry, *J. Phys. Chem. A*, 2020, **124**, 6511–6520.

64 M. Chrayteh, E. Burevschi, D. Loru, T. R. Huet, P. Dréan and M. E. Sanz, Disentangling the complex network of non-covalent interactions in fenchone hydrates via rotational spectroscopy and quantum chemistry, *Phys. Chem. Chem. Phys.*, 2021, 20686–20694.

65 E. M. Neeman, J. R. Aviles Moreno and T. R. Huet, Gas-phase hydration of nopinone: The interplay between theoretical methods and experiments unveils the conformational land-scape, *Phys. Chem. Chem. Phys.*, 2021, **23**, 18137–18144.

66 M. Chrayteh, T. R. Huet and P. Dréan, Microsolvation of myrtenal studied by microwave spectroscopy highlights the role of quasi-hydrogen bonds in the stabilization of its hydrates, *J. Chem. Phys.*, 2020, **153**, 104304.

67 Å. M. Jonsson, M. Hallquist and E. Ljungström, Impact of humidity on the ozone initiated oxidation of limonene, Δ3-carene, and α-pinene, *Environ. Sci. Technol.*, 2006, **40**, 188–194.

68 C. S. Maksymiuk, C. Gayahtri, R. R. Gil and N. M. Donahue, Secondary organic aerosol formation from multiphase oxi-dation of limonene by ozone: Mechanistic constraints via two-dimensional heteronuclear NMR spectroscopy, *Phys. Chem. Chem. Phys.*, 2009, **11**, 7810–7818.

26538 | *Phys. Chem. Chem. Phys.*, 2022, **24**, 26529–26538

This journal is © the Owner Societies 2022